The Role of Sodium Sulfate Supporting Electrolyte in Ammonium Transport and Reduction at Interface Between Platinum Cathode and Solution

Linji Xu[1*], Yunsong Pang[2], Dezhao Huang[2], Huichuan Zhuang[3], Wenzong Liu[4], Tengfei Luo[2], Po-Heng Lee[5], Li Feng[1], Junchi Lu[6]

[1]Environmental Engineering Technology Research Center, Chongqing Academy of Ecology and Environmental Sciences,

Qishan Road 252, Yubei district, Chongqing, P. R. China.

[2]Department of Aerospace and Mechanical Engineering, University of Notre Dame, Notre Dame, Indiana 46556, United States

[3]Department of Civil and Environmental Engineering, The Hong Kong Polytechnic University, Hung Hom, Kowloon, Hong Kong SAR, P. R. China.

[4]Key Laboratory of Environmental Biotechnology, Research Center for Eco-Environmental Sciences, Chinese Academy of Sciences, Beijing 100085, China

[5]Department of Civil and Environmental Engineering, Imperial College London, London, U.K.

[6]Department of Electrical Engineering, University of Notre Dame, Notre Dame, Indiana 46556, United States

[*]Corresponding author: dophegood@gmail.com; phone: +86-88521315

Abstract

Ammonium is a potential hydrogen fuel and can be recovered from high ammonium wastewater via electrodeionization (EDI) process. Since NH_4^+ is a weak acid ion, sodium sulfate (Na_2SO_4) is used as a supporting electrolyte to improve electrolyte's conductivity. This manuscript investigated the NH_4^+ behaviors in high Na_2SO_4 solution through electrochemical analysis methods and molecular dynamics (MD) simulations. Ionic strength increased, leading to a decreased ionic activity, and thus negatively influenced NH_4^+ transportation with the increasing concentration of Na_2SO_4 solution. Na^+ competitively occupied the place of electric double layer (EDL) and impeded NH_4^+ to get closer to the electrode surface. Besides, water molecules played a critical role in determining the net charge density and the potential drop. The experimental tests and theoretical simulation demonstrated that NH_4^+ reduction ($NH_{4\,(aq)}^{+} + e^{-} \rightarrow 0.5H_{2(g)} + NH_{3(g)}$) in the cathode was strengthened in the low concentration range (0-0.25 M Na_2SO_4) but inhibited in the concentration range of 0.5-1.5 mol L^{-1}.

Keywords Supporting electrolyte concentration, Ammonium transport and reduction, Electric double layer, Molecular dynamic simulation

1 Introduction

The concentrated ammonium existing in wastewater and landfill leachate can be recovered as ammonia and hydrogen gas via electrodeionization (EDI) [1]. NH_3 generation has two paths: (1) NH_4^+ is reduced to proton and NH_3 via a one-electron transfer process in the EDI cathode (Eq. 1) [2]; (2) Water splits into OH^- that reacts with NH_4^+ to generate NH_3 (Eq.2 and Eq.3) [3]. NH_4^+ reduction is more likely to occur other than water splitting when EDI is process operated at the low applied voltage (<1.23 V).

$$NH_{4\,(aq)}^{+} + e^{-} \rightarrow \left[NH_4^0\right]_{ads} \rightarrow H_{ads} + NH_{3(aq)} \rightarrow 0.5H_{2(g)} + NH_{3(g)} \quad (1)$$

$$H_2O_{(l)} + e^{-} \rightarrow OH^{-}{}_{(aq)} + 0.5H_{2(g)} \quad (2)$$

$$NH_{4\,(aq)}^{+} + OH^{-}{}_{(aq)} \rightleftharpoons NH_3 \cdot H_2O_{(aq)} \rightleftharpoons NH_{3(g)} + H_2O_{(l)} \quad (3)$$

During NH_4^+ reduction, slow mass transfer determines the generation of NH_3 gas since NH_4^+ is a weak acid ion. To solve this issue, a strong electrolyte such as sodium sulfate is usually added as the supporting electrolyte to enhance electrolyte's conductivity [2, 4-9]. However, the added co-ion often provokes a competition with the target ion. As reported by Casadellà *et al*. who studied the cation completion of K^+, Na^+ and NH_4^+ in urine through polymer inclusion membranes, the order of selective recovery ($K^+ > Na^+ > NH_4^+$) and two-fold flux in Na^+ (4.5×10^{-3} mmol cm^{-2} h^{-1}) over NH_4^+ (1.5×10^{-3} mmol cm^{-2} h^{-1}) was observed [10]. Liu *et al*. conducted a study on the competitive transport of Na^+ and NH_4^+ in bioelectrochemical systems and concluded that Na^+ in anolyte facilitated the transport of NH_4^+ due to the Donnan equilibrium at cation exchange membrane-anolyte/catholyte interfaces [9]. Rosasco *et al*. investigated cation competition in the electrical double layer

(EDL) at a well-defined Pt (111) electrode surface and found the strength order of cation retention, $Na^+ > NH_4^+$, which might be related to the hydrated radius of Na^+ (3.58 Å) over that of NH_4^+ (3.31 Å) weakening electrochemical activities, e.g., charge density, dielectric constant, and rate capability [11-15]. Besides, some researchers reported that the accumulated Na^+ attracted to water molecules and built a compacted Na^+-H_2O layer, which deterred the electrochemical reaction kinetics [16, 17]. Others depicted that Na^+ competitively reduced the effective current efficiency of NH_4^+ and produced electrode overpotential at a fixed electric current [18-21]. Therefore, the influences of Na^+ on the behaviors of mass transportation in the EDL cannot be ignored when Na_2SO_4 is used as the supporting electrolyte.

Mass transportation in the EDL is investigated through theoretical simulation other than experimental tests due to the measuring difficulties of the transport coefficient and mass quantification. The classical theories of the mass distribution in the EDL includes Fick's diffusion laws, Nernst-Planck, and Nernst-Einstein equation. The latest theoretical simulations such as molecular dynamics (MD) simulations built on EDL theories are increasingly popular because simulations from the molecular level can deliver insightful information about the interactions at the electrode interface. For instance, Soroosh and Hai conducted MD simulations of flexible-boundary Quantum Mechanics/Molecular Mechanics to reveal ion solvation and found that NH_4^+ had a more significant discrepancy in the extent of charge transfer (by about 0.3 e^-) and more extensive distribution than Na^+ (0.1 e-) [12]. Soetardji *et al*. used the Langmuir model to study NH_4^+ removal from wastewater via sodium hydroxide modified zeolite mordenite and found that the

44 competition from Na^+ decreased the removal efficiency of NH_4^+ through the different
45 reaction mechanisms [21]. To date, however, NH_4^+ transport at the interface of Pt-
46 solution under the different gradients of Na^+ concentration has not yet been well studied.
47 The objective of this study is to understand the mechanism of supporting electrolyte
48 concentration affecting NH_4^+ behavior and provide the opportunity to elucidate the
49 related molecular-level mechanism. Therefore, we employed electrochemical tests
50 combined with MD simulations to examine the effects of Na_2SO_4 concentration on NH_4^+
51 migration, reduction, and electric properties of the cathodic EDL.

52 **2 Experimental tests and theoretical calculation**

53 2.1 Experimental tests

54 *Equipment setup.* Figure 1 shows the configuration of a sandwich-type EDI stack. The
55 working volume is 40.0 cm^3: 60.0 mm × 60.0 mm × 11.0 mm, in which the 11.0 mm
56 included a 10.0 mm distance between the anode and the cathode and 1.0 mm thick
57 silicone gaskets. The electrodes were titanium plates coated in a 0.02 mm thick layer of
58 platinum, with a 16.0 cm^2 effective area. The original electrolyte was 0.25 M ammonium
59 sulfate, which was then mixed with 0–1.5 M sodium sulfate supporting electrolyte at a
60 25.0 °C operating temperature. The conductivity was measured with a conductivity meter
61 (Shanghai Leici-Chuangyi Instrument and Meter Co., Ltd).

62 *Cyclic voltammetry scanning.* The tests of current density versus applied voltage were
63 carried out using the EDI stack as described above. The scanning electrolyte was the

mixtures of fixed ammonium sulfate (0.25 M) and changed the concentration of sodium sulfate (0.125-1.5 M). The reference electrode was Ag/AgCl-217 (INESA Scientific InstrumentCo., Ltd) that has a double-salt bridge. The current was recorded and analyzed by the electrochemical working station (CorrWare®, Scribner Associates Inc., U.S.A.), as shown in Figure 1.

2.2 Computational methods

Electrode/electrolyte interface modeling. The simulation system was a three-dimensional supercell with periodic boundary conditions, constructed in the Materials Studio software. It was composed of Pt sheets (50 Å × 50 Å) as electrodes and the electrolyte aligned in parallel with an interlayer distance of 140 Å, shown in Figure SI-1(a). To simulate the Pt electrode/electrolyte interface, water molecules and NH_4^+ with different concentrations of Na^+ and SO_4^{2-} were added to the space between anode and cathode. Both anode and cathode were Pt (100) surface consisting of 338 atoms, 7 layers for each pole. The numbers of the atoms of the Pt-solution system are summarized in Table SI-1 and Table SI-2.

Equilibrium relaxation and data collection. MD simulations were performed using the Atomic/Molecular Massively Parallel Simulator package (LAMMPS) at a temperature of 300 K and a pressure of 1 atm [3, 22]. The interatomic interactions were simulated using Lennard-Jones (LJ) potential as described in Eq. 4:

$$E = 4\xi_{LJ}\left[\left(\frac{d_{LJ}}{r}\right)^{12} - \left(\frac{d_{LJ}}{r}\right)^{6}\right] \quad (4)$$

Where ξ_{LJ} and d_{LJ} are the respective parameters of energy and length, as summarized in Table SI-2. The electrostatic interaction between charged atoms was calculated using Coulomb's law (Eq. 5) with the Coulombic interactions computed using the particle-particle particle-mesh (PPPM) algorithm [23].

$$E = \frac{Cq_1q_2}{\varepsilon r} \quad (5)$$

where C is an energy-conversion constant, q_1 and q_2 are the charges carried by two atoms, ε is the dielectric constant. Bonds and angles among atoms are held rigid using the SHAKE algorithm [24]. Water molecules are simulated using the rigid SPC/E water model and the Pt atoms are held fixed [25]. The NVT ensemble simulations were carried out at 300 K with Langevin thermostats for 1.0 ns with a 0.5 fs time step size. NPT ensemble simulations at 1 atm and 300 K were then carried out.

After the systems reaching the thermal equilibrium state, we collected data (i.e., mass density, number density, mean square displacement (MSD), radial distribution function (RDF), etc.) during an NVE ensemble for 0.5 ns, as displayed in Figure SI-1(b) and Figure SI-1(c). A voltage of 3.0 V was applied to the solution by applying the corresponding electrostatic forces $F = qE$ on each charged atom. For post-processing the results, the channel was split into a set of bins (1.0 Å in width) along the direction (x) perpendicular to the Pt surface. The mass density $\rho(x)$ was then used to analyze the EDL structures.

2.3 Data analysis

Charge density. Charge density is an important property for analyzing EDL. According to the axial number density of atoms, the total charge density profile, $\sigma_{q(x)}$, is contributed by ions and water, as expressed in Eq. 6.

$$\sigma_{q(x)} = \sum_{i \ni surf} \sigma_i(x) q_i + \sigma_O(x) q_O + \sigma_H(x) q_H \qquad (6)$$

where σ_i, σ_O, and σ_H are the number densities of ions, water–oxygen, and water–hydrogen, respectively. q_i, q_O, and q_H are the charges carried by them, respectively.

Electric field and potential profiles. Electric field strength and potential oscillate with variations in charge density. The electric field ($E_{q(x)}$) component normal to the Pt surface was calculated by integrating the net charge density as described by Eq. 7.

$$E_{q(x)} = -(1/\in_0) \int_{-\infty}^{x} \sigma_q(x')(x - x')dx' \qquad (7)$$

The potential was computed by integrating the Poisson equation in one dimension, as described in Eq. 8.

$$\frac{\partial^2 V(x)}{\partial x^2} = -\frac{\sigma(x)}{A_{Pt}\varepsilon_0} \qquad (8)$$

where $\sigma(x)$, A_{Pt}, and ε_0 are the net charge density, the size of the Pt sheet and the vacuum dielectric constant, respectively. Eq. 8 was numerically integrated to obtain $V(x)$, as shown in Eq. 9 using $x=L/2$ (the middle of the channel) as a reference that was regarded as zero charge density (Eq. 9).

$$V(x) = \int\int_{L/2}^{x} \frac{\sigma(x)}{A_G \varepsilon_0} dx^2 \quad (9)$$

Mean square displacement (MSD). MSD is expressed by R^2 that is a measure of the length of the path of a molecule traveled. It is directly related to the diffusion coefficient of this molecule through Einstein's equation [26]. As a result, MSD can be used to gain insight into transport phenomena [27]. MSD in MD simulation can be calculated as:

$$R^2 \equiv \left\langle \left(x - x_0\right)^2 \right\rangle = \frac{1}{N} \sum_{n=1}^{N} \left(x_n\left(t\right) - x_n\left(0\right)\right)^2 \quad (10)$$

where N is the number of particles to be averaged, $x_n(0)=x_0$ is the reference position of each particle, and $x_n(t)$ is the position of each particle at time, t. By tracking the molecular positions, the MSD of the particles was calculated to quantify ion and water transport in the EDL.

Diffusion coefficient. The diffusion coefficient is the rate of mass transport, as described by the slope (r) of the *MSD* versus *t* curves (Eq. 11) from Einstein's equation.

$$D = \lim_{t \to \infty} \frac{1}{6t} \left\langle \left[r\left(t\right) - r\left(0\right) \right]^2 \right\rangle \quad (11)$$

where r and t are atomic compound position and time, respectively.

Radial distribution function (RDF). RDF is defined as Eq. 12.

$$g(r) = \rho(r) / \rho \quad (12)$$

where $\rho(r)$ is the local number density of atoms at a given radius; ρ is the average mass of the whole solution.

3 Results and discussion

3.1 Ion transport in interfacial solution via experimental tests

3.1.1 Solution properties

The influence of Na_2SO_4 concentration on ion strength and activity coefficient [28, 29] of NH_4^+ (z_i=1, a_i^0=0.3 and b_i=0.2) was plotted (Figure 2(a)). The ion strength is strengthened from 1.0 M at 0.125 M Na_2SO_4 to 5.5 M at 1.5 M Na_2SO_4. However, the activity coefficient of NH_4^+ goes down from 0.3 to 0.05, signifying that the increased concentration of supporting electrolyte negatively affected the activity of NH_4^+. The concentration also influenced pH value and conductivity. As shown in Figure 2(b), pH value experiences a sharp increase as the concentration of Na_2SO_4 solution below 0.5 M but a smooth increase to 9.99 at 1.5 M, indicating that increasing the concentration of Na_2SO_4 solution does not bring an apparent effect on pH value in the concentrated range.

3.1.2 Ion migration

The changed characteristics caused by ion strength and activity impacts ion transport in the interfacial solution. Ion migration can be described through viscosity and mobility. Viscosity calculated based on Jones-Dole`s equation [30-32] experiences a slow growth from 80 mPas below 0.25 M, and a sharp climb to 330 mPas at 1.5 M. The visible increase in dynamic viscosity reflects that increasing concentration lowers the liquidity of bi-electrolyte so that produces a high resistance to ion migration (Figure SI-2). The variations of ion mobility and number calculated according to $\mu=ez/6\pi\eta r$ [33] were

summarized in Table 1. NH_4^+ has an increase in mobility from 1.01 $m^2 V^{-1} s^{-1}$ to 1.49 $m^2 V^{-1} s^{-1}$ at 0.125 M, but a drop to 1.27 $m^2 V^{-1} s^{-1}$ at 1.5 M. Na^+ and SO_4^{2-} have drops to 1.63 $m^2 V^{-1} s^{-1}$ and 0.81 $m^2 V^{-1} s^{-1}$, respectively. Concerning transport number, both NH_4^+ and SO_4^{2-} decreases from 0.17 and 0.5 at 0.125 M to 0.08 and 0.28 at 1.5 M, respectively. However, Na^+ increases to 0.64 at 1.5 M. The results of ion transport reveal that the large hindrance may lead to the lack of NH_4^+ as an electron carrier at the cathode interface, which has been elaborated by Pal [16].

3.2 Ion transport in electric double layer via MD simulation

3.2.1 Ion diffusion coefficient

Due to the limitation of experimental detection, the diffusion coefficient was elaborated using MD simulation. The migrations of NH_4^+ and Na^+ in the EDL were quantified via the MSD values of N and Na atoms. The average MSD slope of the N atoms grows from 2.1874 $\times 10^3$ at 0 M to 3.1687 $\times 10^3$ at 0.25 M but drops to 1.457 $\times 10^3$ at 1.5 M in 0–1.5 M Na_2SO_4 and as a function of time of 0.5 ns (Table SI-3). The corresponding diffusion coefficient of NH_4^+ increases from 2.1874 $\times 10^{-9}$ $m^2 s^{-1}$ at 0 M to 5.2812 $\times 10^{-9}$ $m^2 s^{-1}$ at 0.25 M but falls to 2.4319 $\times 10^{-9}$ $m^2 s^{-1}$ at 1.5 M as displayed in Figure 3(a) and Figure 3(b). The largest diffusion coefficients are obtained at 0.25 M. For the over-concentrated Na_2SO_4 electrolyte (> 0.5 M), the diffusion coefficient of Na^+ is smaller than that of NH_4^+, meaning that the concentrated Na^+ does not only impede NH_4^+ migration but also influence it self-transport. For the dilution, the trend of the diffusion coefficient can be explained by the

Nernst-Einstein equation that establishes the relationship between the molar limiting conductivity ($\Lambda_{m,i}^0$) and the diffusion coefficient D_i [34].

$$D_i = \frac{RT}{z_i^2 F^2} \Lambda_{m,i}^0 \qquad (13)$$

where z_i, T, F, and R are charge number of ion i, absolute temperature, Faraday's constant, and the ideal gas constant, respectively. The diffusion coefficients linearly rely on the molar limiting conductivity ($\Lambda_{m,i}^0$). However, this formula becomes more complicated for the concentrated solution. The diffusion coefficient is also related to the trajectories of the particle [35]. Namely, the decreases of diffusion coefficients may be caused by the charge neutralization in OHP [36, 37]. Apart from Na^+ and NH_4^+, water molecular should not be ignored since the H-H bond effect on the electronic structure is essential for understanding the physical and chemical properties of the EDL [38, 39]. From the calculated results of average MSD slope of water molecules using Einstein's equation, its diffusion coefficient of D_{water}, 7.5×10^{-9} m^2 s^{-1} indicates that water molecules have the largest migration coefficient (Figure SI-3). This trend is because the self-diffusion and interdiffusion coefficients decrease with an increase of salt concentration and water molecules in pure water diffuse faster than in concentrated electrolyte. Our simulation results are in good agreement with the study conducted by Kong et al. and Lyubartsev and Laaksonen [40, 41]. Therefore, the order of diffusion constants of NH_4^+, Na^+ and water is $D_{water} > D_{Na+} > D_{NH4+}$ in the diluted concentration, and $D_{water} > D_{NH4+} > D_{Na+}$ in the concentrated Na_2SO_4 solution.

3.2.2 Ion concentration distribution

The concentration distribution was described with mass density calculated via the mass coordinate. Figure 4 shows the distributions of the mass density of NH_4^+ and Na^+ along the x-axis near the cathodic surface. Specifically, NH_4^+ density increases to the most significant peak (0.016 g cm^{-3}), which is a compacted charge layer called the inner Helmholtz plane (IHP) in the region nearest to the Pt surface [42, 43]. As the distance extending to the bulk solution, NH_4^+ density displays the second peak (0.007 g cm^{-3}, on average) that is considered the outer Helmholtz plane (OHP). When the distance extends further away from the Pt surface, NH_4^+ density stabilizes at 0.0045 g cm^{-3} in Figure 4(b), which is regarded as the diffusion layer (DL) [44]. The distribution profile of Na^+ has similar peaks to that of NH_4^+ along the x-axis (Figure 4(d)), whereas the peak of Na^+ closest to the Pt surface increases from 0 g cm^{-3} at 0 M to 0.018 g cm^{-3} at 1.5 M with the bulk Na_2SO_4 electrolyte concentrate. The comparison of the concentration distribution of NH_4^+ and Na^+ in Figures 4(c) and 4(d) shows that the NH_4^+ density reduces from 0.016 g cm^{-3} to 0.003 g cm^{-3}, which is significantly lower than that of Na^+ at the corresponding concentration. The difference in the concentration distributions of NH_4^+ and Na^+ may depend on the diffusion coefficient since the diffusion coefficient of NH_4^+ is smaller than that of Na^+. Additionally, the concentration profiles of NH_4^+ and Na^+ indicate that the lowered peak of NH_4^+ is caused by the competitive increase of Na^+ concentration, especially in the over-concentrated Na_2SO_4 electrolyte (>0.5 M). The phenomena above are related to the transient repulsion of ammonium ($[NH_4^{0\cdot}]_{ads}$) and Na-H_2O hydration "atmosphere" [45].

3.2.3 Ion charge density and EDL thickness

Ion transportation and accumulation forms an EDL around the electrodes. Figure 5(a) and 5(b) illustrates the charge density profiles and the potential drop of NH_4^+ and Na^+ in the range of 0–1.5 M. There are two remarkable peaks (0.0009 e $Å^{-3}$ and 0.0004 e $Å^{-3}$) referring to the IHP and OHP of the NH_4^+ charge density curve, in which the value of NH_4^+ potential changes from -0.0225 V to 0 V (Figure 5(c) and 5(d)). Integrating NH_4^+ charge in the x-axis, the charge density and potential drop of NH_4^+ film decline from 0.0041 e $Å^{-3}$ and -0.0226 V at 0 M to 0.0006 e $Å^{-3}$ and -0.0151 V at 1.5 M, respectively, as summarized in Table 2. Na^+ charge density increases and the potential escalating. However, the film of Na^+ peaks disappear as Na_2SO_4 becomes over-concentrated.

All atoms with different charge always interact with each other in the aqueous condition. Due to the negative charge carried by O in the H_2O molecule, the total charge density and potential drop shift from 0.0011 e $Å^{-3}$ and 0.0095 V to -0.0228 e $Å^{-3}$ and -0.0449 V, respectively, (Figure SI-5 and Table 2). The variation of net charge density indicates the importance of water molecule. As studied by Guo et al., water molecule at the interface between the solution and electrodes forming hydrogen bonding changed the local electronic structure of EDL [38]. The results gained by Velasco-Velez et al. elucidates that the inert electrode surface can induce water molecules when the electrode is negatively charged and therefore attracting the more positive H atoms [46].

Based on the total charge density and potential drop, the thicknesses of the NH_4^+ layer and Na^+ layer as the function of Na_2SO_4 concentration are calculated and summarized in

Table 3. The total thickness of NH_4^+ EDL experiences a slight increase from 19.0 Å at 0 M to 21.0 Å at 1.5 M but an apparent decrease to 16.0 Å at 1.5 M. In the Na_2SO_4, the IHP declines to 4.0 Å from 6.0 Å; the OHP increases to 8.5 Å at 0.25 M but decreases to 6.5 Å at 0.25 M; and DL varies from 5.5 to 7.0 Å. The comparison of IHP, OHP, and DL discloses that Na_2SO_4 concentration has a greater influence on the Helmholtz layer (IHP and OHP) than DL. The total thickness of Na^+ increases from 0 Å at 0 M to 23.5 Å at 1.5 M. The HP is thicker than the DL. These variations are mainly attributed to the excess accumulation of ions from the diffusion layer and the insufficient supply of ions in the bulk solution [15, 47, 48]. Taking the thickness overlap of NH_4^+ and Na^+ into consideration, the total EDL thickness increases from 19.5 Å at 0 M to 23.5 Å at 1.5 M. According to the Debye–Hückel equation, the charge density of Na^+ adsorption causes an increase of the Na^+ layer [49]. Therefore, the thick Na^+ layer blocks the rate of electron transfer of NH_4^+ reduction so that the lack of an electron acceptor results in the decrease of the current density peak of NH_4^+ reduction.

3.3 Ammonium reduction

The differences of electric properties in charge density, potential drop, capacitance, and thickness can reflect the kinetics of ion oxidation/reduction. To exam NH_4^+ reduction at the cathode interface of EDI, current-voltage and generated gas were measured. The current-voltage curves were obtained at a 10.0 mV s^{-1} scanning rate under 0–1.5 M Na_2SO_4 as supporting electrolyte (Figure 6). A single peak in the range of 0-0.8 V applied voltage was observed on each curve. For forward scanning, the current density increases to 0.005 mA cm^{-2} with Na_2SO_4 concentration increasing to 0.5 M from 0 M. However, the

forward current density does not continuously increase although the concentration of Na_2SO_4 increases to 1.5 M. For backward scanning, the peak current decreases from -0.023 mA cm^{-2} to -0.005 mA cm^{-2}, moving to the positive y-axis as the bulk Na_2SO_4 electrolyte concentrating at 0.23 V (Figure 6(a)). The results are constant with that of the experimental tests.

The generated gas was analyzed through gas chromatography and quantified through the mass of nitrogen element. The plot shows that the mass in the liquid (anodic and cathodic) is dominant, ammonia nitrogen takes second place and nitrogen gas is tiny (Figure 6(b)). The changes of anodic-N and cathodic-N are because of migration. NH_3 and N_2 gas are from NH_4^+ reduction (Eq.1) and base neutralization (Eq.2 and Eq.3).

NH_4^+ reduction experiences the absorption of intermediates, $[NH_4^0]_{ads}$ and H_{ads}. $[NH_4^0]_{ads}$, adsorbed Rydberg radicals and repulsed NH_4^+ solvent molecules approaching for additional binding so that the accumulation of $[NH_4^0]_{ads}$ in the EDL leads to the NH_4^+ concentration reducing [50-54].

$$NH_{4\,(aq)}^{+} + e^{-} \rightarrow \left[NH_4^0\right]_{ads} \tag{14}$$

$$\left[NH_4^0\right]_{ads} \rightarrow NH_3^{*} + H_{ads} \tag{15}$$

$$NH_3^{*} \rightarrow NH_2^{*} + H_{ads} \tag{16}$$

$$\vdots$$

$$2N^{*} \rightarrow N_2 + 2^{*} \tag{17}$$

where * is an active site.

The first step is dominant, and the flowing steps process slowly so that the mass of nitrogen gas is little. As integrating the experimental and theoretical results, we find that the increase of the concentration of Na_2SO_4 electrolyte changes the current density of ammonium reduction (from -0.023 mA cm^{-2} to -0.005 mA cm^{-2} at 0.23 V).

4 Conclusion

This paper discussed the effects of Na_2SO_4 supporting electrolyte from 0 M to 1.5 M on NH_4^+ reduction in the cathode surface of EDI using electrochemical analysis and MD simulations. The results demonstrate that increasing the concentration of Na_2SO_4 supporting electrolyte enhances the conductivity and total current but reduces ion activity. The migration rates of NH_4^+ and Na^+ increase in the dilute range (0-0.25 M) but a decrease in the concentrated range (>0.5 M). The fierce competitive adsorption of Na^+ forming a thick layer blocks NH_4^+ migration and electron transportation in the EDL. NH_4^+ reduction is weakened with the increase of Na_2SO_4 supporting electrolyte. Interestingly, water molecules play a critical role in determining the net charge density and potential drop. Therefore, the mechanisms presented in this manuscript disclose the function of the co-ion concentration and the results can allow the manipulation of EDI capacity optimization.

5 Acknowledgements

We acknowledge the support of various grants, including the Chongqing Science and Technology Bureau (cstc2018jszx-zdyfxmX0016), Chongqing Ecology and Environment Bureau (2019-89) for providing financial support.

6 References

[1] L. Xu, F. Dong, H. Zhuang, W. He, M. Ni, S.P. Feng, P.H. Lee, Energy upcycle in anaerobic treatment: Ammonium, methane, and carbon dioxide reformation through a hybrid electrodeionization–solid oxide fuel cell system, Energy Conversion and Management 140 (2017) 157-166.

[2] O. Berkh, Y. Shacham-Diamand, E. Gileadi, Reduction of ammonium ion on Pt electrodes, Journal of The Electrochemical Society 155(10) (2008) F223-F229.

[3] D.J. Little, M.R. Smith III, T.W. Hamann, Electrolysis of liquid ammonia for hydrogen generation, Energy & Environmental Science 8(9) (2015) 2775-2781.

[4] E. Simons, E. Cairns, D. Surd, The performance of direct ammonia fuel cells, Journal of The Electrochemical Society 116(5) (1969) 556-561.

[5] L. Xu, F. Dong, H. Zhuang, W. He, M. Ni, S.-P. Feng, P.-H. Lee, Energy upcycle in anaerobic treatment: Ammonium, methane, and carbon dioxide reformation through a hybrid electrodeionization–solid oxide fuel cell system, Energy Conversion and Management 140 (2017) 157-166.

[6] L. Alvarado, A. Chen, Electrodeionization: principles, strategies and applications, Electrochimica Acta 132 (2014) 583-597.

[7] S.-H. Moon, S.-H. Yun, Process integration of electrodialysis for a cleaner environment, Current Opinion in Chemical Engineering 4 (2014) 25-31.

[8] I. Wenten, K. Khoiruddin, P. Aryanti, A. Hakim, Scale-up Strategies for Membrane-Based Desalination Processes: A Review, Journal of Membrane Science and Research 2(2) (2016) 42-58.

[9] M.P. Mousavi, B.E. Wilson, S. Kashefolgheta, E.L. Anderson, S. He, P. Bu¨hlmann, A. Stein, Ionic Liquids as Electrolytes for Electrochemical Double-Layer Capacitors: Structures that Optimize Specific Energy, ACS Applied Materials & Interfaces 8(5) (2016) 3396-3406.

[10] J. Goodenough, H. Abruna, M. Buchanan, Basic Research Needs for Electrical Energy Storage. Report of the Basic Energy Sciences Workshop on Electrical Energy Storage, April 2-4, 2007, DOESC (USDOE Office of Science (SC)), 2007.

[11] E.J. Olson, P. Bühlmann, Unbiased Assessment of Electrochemical Windows: Minimizing Mass Transfer Effects on the Evaluation of Anodic and Cathodic Limits, Journal of The Electrochemical Society 160(2) (2013) A320-A323.

[12] A. Casadellà, O. Schaetzle, K. Nijmeijer, K. Loos, Polymer inclusion membranes (PIM) for the recovery of potassium in the presence of competitive cations, Polymers 8(3) (2016) 76.

[13] Y. Liu, M. Qin, S. Luo, Z. He, R. Qiao, Understanding ammonium transport in bioelectrochemical systems towards its recovery, Scientific Reports 6 (2016).

[14] S.D. Rosasco, J.L. Stickney, G.N. Salaita, D.G. Frank, J.Y. Katekaru, B.C. Schardt, M.P. Soriaga, D.A. Stern, A.T. Hubbard, Cation competition in the electrical double-layer at a well-defined electrode surface Li+, Na+, K+, Cs+, H+, Mg2+, Ca2+, Ba2+, La3+, tetramethylammonium, choline and acetylcholine cations at Pt (111) surfaces containing an ordered layer of cyanide, Journal of Electroanalytical Chemistry And Interfacial Electrochemistry 188(1-2) (1985) 95-104.

[15] C. Cagle, G. Feng, R. Qiao, J. Huang, B.G. Sumpter, V. Meunier, Structure and charging kinetics of electrical double layers at large electrode voltages, Microfluidics and Nanofluidics 8(5) (2010) 703-708.

[16] G. Jiang, C. Cheng, D. Li, J.Z. Liu, Molecular dynamics simulations of the electric double layer capacitance of graphene electrodes in mono-valent aqueous electrolytes, Nano Research 9(1) (2016) 174-186.

[17] A. Yoshida, K. Imoto, Electric double layer capacitor and method for producing the same, Google Patents, 1992.
[18] S. Yoon, J.H. Jang, H.K. Bok, S.M. Oh, Complex capacitance analysis on rate capability of electric-double layer capacitor (EDLC) electrodes of different thickness, Electrochimica Acta 50(11) (2005) 2255-2262.
[19] M. Vossen, F. Forstmann, Integral equation theory for the electrode-electrolyte interface with the central force water model. Results for an aqueous solution of sodium chloride, Molecular Physics 86(6) (1995) 1493-1516.
[20] Z. Ma, M. Wang, X. Gao, C. Gao, Charge and separation characteristics of nanofiltration membrane embracing dissociated functional groups, Frontiers of Environmental Science & Engineering 8(5) (2014) 650-658.
[21] S. Alexey, M. Jr, A. D, Competition among Li+, Na+, K+, and Rb+ monovalent ions for DNA in molecular dynamics simulations using the additive CHARMM36 and Drude polarizable force fields, The Journal of Physical Chemistry B 119(12) (2015) 4428-4440.
[22] P. Soroosh, L. Hai, Molecular dynamics simulations of ion solvation by flexible-boundary QM/MM: On-the-fly partial charge transfer between QM and MM subsystems, Journal of Computational Physics 35(24) (2014) 1778-1788.
[23] J.P. Soetardji, J.C. Claudia, Y.-H. Ju, J.A. Hriljac, T.-Y. Chen, F.E. Soetaredjo, S.P. Santoso, A. Kurniawan, S. Ismadji, Ammonia removal from water using sodium hydroxide modified zeolite mordenite, Rsc Advances 5(102) (2015) 83689-83699.
[24] L. Joly, C. Ybert, E. Trizac, L. Bocquet, Hydrodynamics within the electric double layer on slipping surfaces, Physical Review Letters 93(25) (2004) 257805.
[25] J.W. Lee, J.A. Templeton, K.K. Mandadapu, J.A. Zimmerman, Comparison of molecular and primitive solvent models for electrical double layers in nanochannels, Journal of Chemical Theory and Computation 9(7) (2013) 3051-3061.
[26] S. Plimpton, Fast parallel algorithms for short-range molecular dynamics, Journal of Computational Physics 117(1) (1995) 1-19.
[27] J.-P. Ryckaert, G. Ciccotti, H.J. Berendsen, Numerical integration of the cartesian equations of motion of a system with constraints: molecular dynamics of n-alkanes, Journal of Computational Physics 23(3) (1977) 327-341.
[28] D.A. Skoog, D.M. West, F.J. Holler, S. Crouch, Fundamentals of analytical chemistry, Nelson Education2013.
[29] J. Kielland, Individual activity coefficients of ions in aqueous solutions, Journal of the American Chemical Society 59(9) (1937) 1675-1678.
[30] A. Alp, A. Nain, N. Kumar, M. Ibrahim, Density and viscosity of magnesium sulphate in formamide+ ethylene glycol mixed solvents, Journal of Chemical Sciences 114(5) (2002) 495-500.
[31] A. Korosi, B. Fabuss, VISCOSITIES OF BINARY AQUEOUS SOLUTIONS OF NACL KCL NA2SO4 AND MGSO4 AT CONCENTRATIONS AND TEMPERATURES OF INTEREST IN DESALINATION PROCESSES, Journal of chemical and engineering data 13(4) (1968) 548-&.
[32] A. Bald, Z. Kinart, R. Tomaš, Viscosity Coefficients of KCl, NaCl, NaI, KNO 3, LiNO 3, NaBPh 4 and Bu 4 NI in Water-Dimethyl Sulfoxide Binary Mixtures With a Low Organic Solvent Content, Croatica Chemica Acta 89(3) (2016) 345-353.
[33] S. Trasatti, Atkins' Physical Chemistry, P. Atkins, J. De Paula, Oxford University Press, Oxford, UK (2006), ISBN: 0198700725, Pergamon, 2007.
[34] D. Frenkel, B. Smit, Understanding molecular simulation: from algorithms to applications, Academic press2001.

[35] D.C. Rapaport, D.C.R. Rapaport, The art of molecular dynamics simulation, Cambridge university press2004.
[36] S.W. Feldberg, On the dilemma of the use of the electroneutrality constraint in electrochemical calculations, Electrochemistry Communications 2(7) (2000) 453-456.
[37] E.M. Ney, Electrical Double Layer Potential Distribution in Nanoporous Electrodes from Molecular Modeling and Classical Electrodynamics Analysis, (2016).
[38] J.-H. Guo, Y. Luo, A. Augustsson, J.-E. Rubensson, C. Såthe, H. Ågren, H. Siegbahn, J. Nordgren, X-ray emission spectroscopy of hydrogen bonding and electronic structure of liquid water, Physical review letters 89(13) (2002) 137402.
[39] P.L. Silvestrelli, M. Parrinello, Structural, electronic, and bonding properties of liquid water from first principles, The Journal of chemical physics 111(8) (1999) 3572-3580.
[40] J. Kong, Z. Bo, H. Yang, J. Yang, X. Shuai, J. Yan, K. Cen, Temperature dependence of ion diffusion coefficients in nacl electrolyte confined within graphene nanochannels, Physical Chemistry Chemical Physics 19(11) (2017) 7678-7688.
[41] A.P. Lyubartsev, A. Laaksonen, Concentration effects in aqueous NaCl solutions. A molecular dynamics simulation, The Journal of Physical Chemistry 100(40) (1996) 16410-16418.
[42] S. Krishnamurthy, P. Bhattacharya, P. Phelan, R. Prasher, Enhanced mass transport in nanofluids, Nano Letters 6(3) (2006) 419-423.
[43] B.N. Pal, B.M. Dhar, K.C. See, H.E. Katz, Solution-deposited sodium beta-alumina gate dielectrics for low-voltage and transparent field-effect transistors, Nature Materials 8(11) (2009) 898.
[44] M. Belonenko, N. Lebedev, S. Sudorgin, Electrical conductivity and diffusion coefficient of electrons in a graphene bilayer, Technical Physics 57(7) (2012) 1025-1029.
[45] H. Lim, W. Lu, X. Chen, Y. Qiao, Effects of ion concentration on thermally-chargeable double-layer supercapacitors, Nanotechnology 24(46) (2013) 465401.
[46] J.-J. Velasco-Velez, C.H. Wu, T.A. Pascal, L.F. Wan, J. Guo, D. Prendergast, M. Salmeron, The structure of interfacial water on gold electrodes studied by x-ray absorption spectroscopy, Science 346(6211) (2014) 831-834.
[47] E.M. Evleth, E. Kassab, Role of Rydberg radicals in electrochemistry, Pure and Applied Chemistry 60(2) (1988) 209-214.
[48] K. Laidler, J. Meiser, B. Sanctuary, Physical Chemistry 2003, Houghton Mifflin: Boston, MA.
[49] N. Kallay, T. Preočanin, D. Kovačević, J. Lützenkirchen, E. Chibowski, Electrostatic potentials at solid/liquid interfaces, Croatica chemica acta 83(3) (2010) 357-370.
[50] M. Morita, T. Kaigaishi, N. Yoshimoto, M. Egashira, T. Aida, Effects of the electrolyte composition on the electric double-layer capacitance at carbon electrodes, Electrochemical and Solid-state Letters 9(8) (2006) A386-A389.
[51] K. Kordesch, J. Gsellmann, M. Cifrain, S. Voss, V. Hacker, R.R. Aronson, C. Fabjan, T. Hejze, J. Daniel-Ivad, Intermittent use of a low-cost alkaline fuel cell-hybrid system for electric vehicles, J. Power Sources 80(1) (1999) 190-197.
[52] N. Dekker, G. Rietveld, Highly efficient conversion of ammonia in electricity by solid oxide fuel cells, J. Compos. Tech. Res. 3(4) (2006) 499-502.
[53] A. Fuerte, R. Valenzuela, M. Escudero, L. Daza, Ammonia as efficient fuel for SOFC, J. Power Sources 192(1) (2009) 170-174.
[54] M. Boudart, G. Djéga-Mariadassou, Kinetics of heterogeneous catalytic reactions, Princeton University Press2014.

Figures

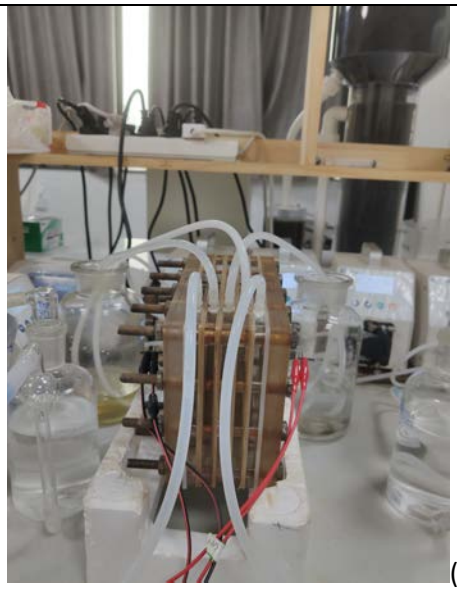

(a)

(b)

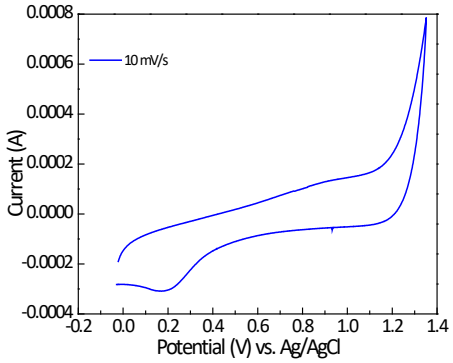

(c)

Figure 1 (a) The experimental set-up; (b) and (c) cyclic voltammetry scanning.

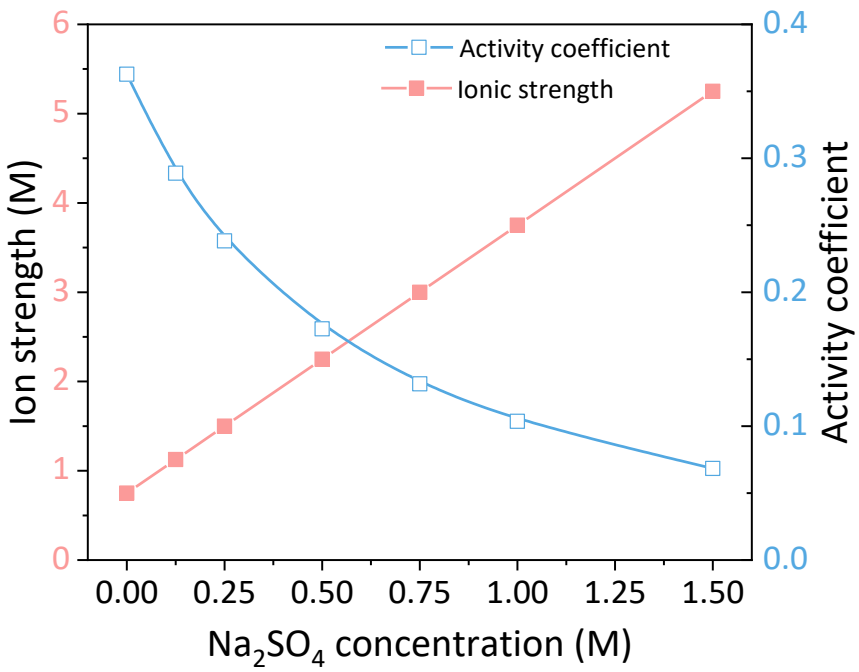

(a)

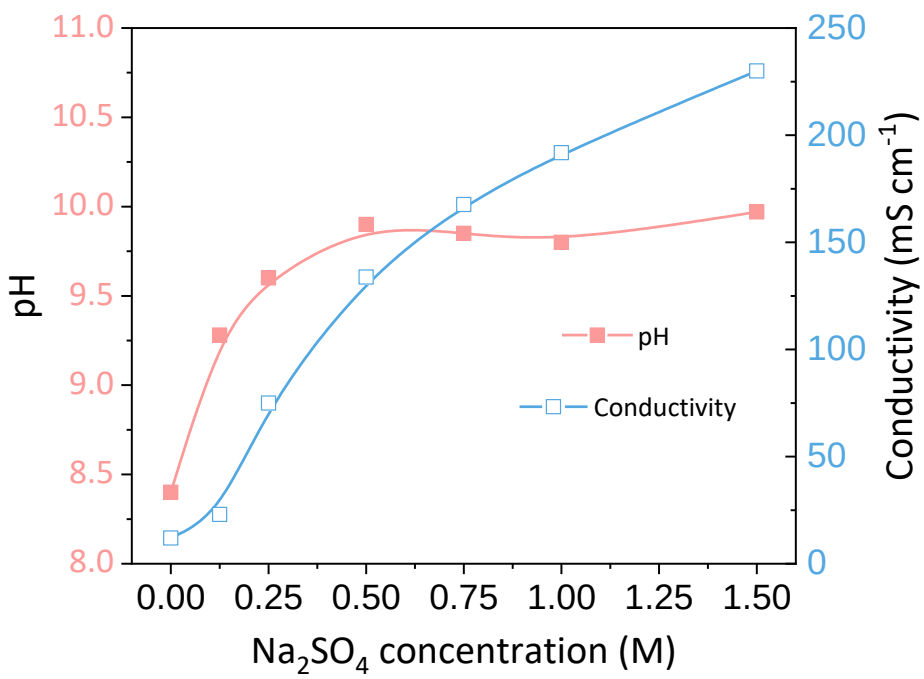

(b)

Figure 2 Characteristics of solution at 0-1.5 M Na_2SO_4 electrolyte. (a)Ion strength and activity coefficient of NH_4^+; (b) pH and conductivity

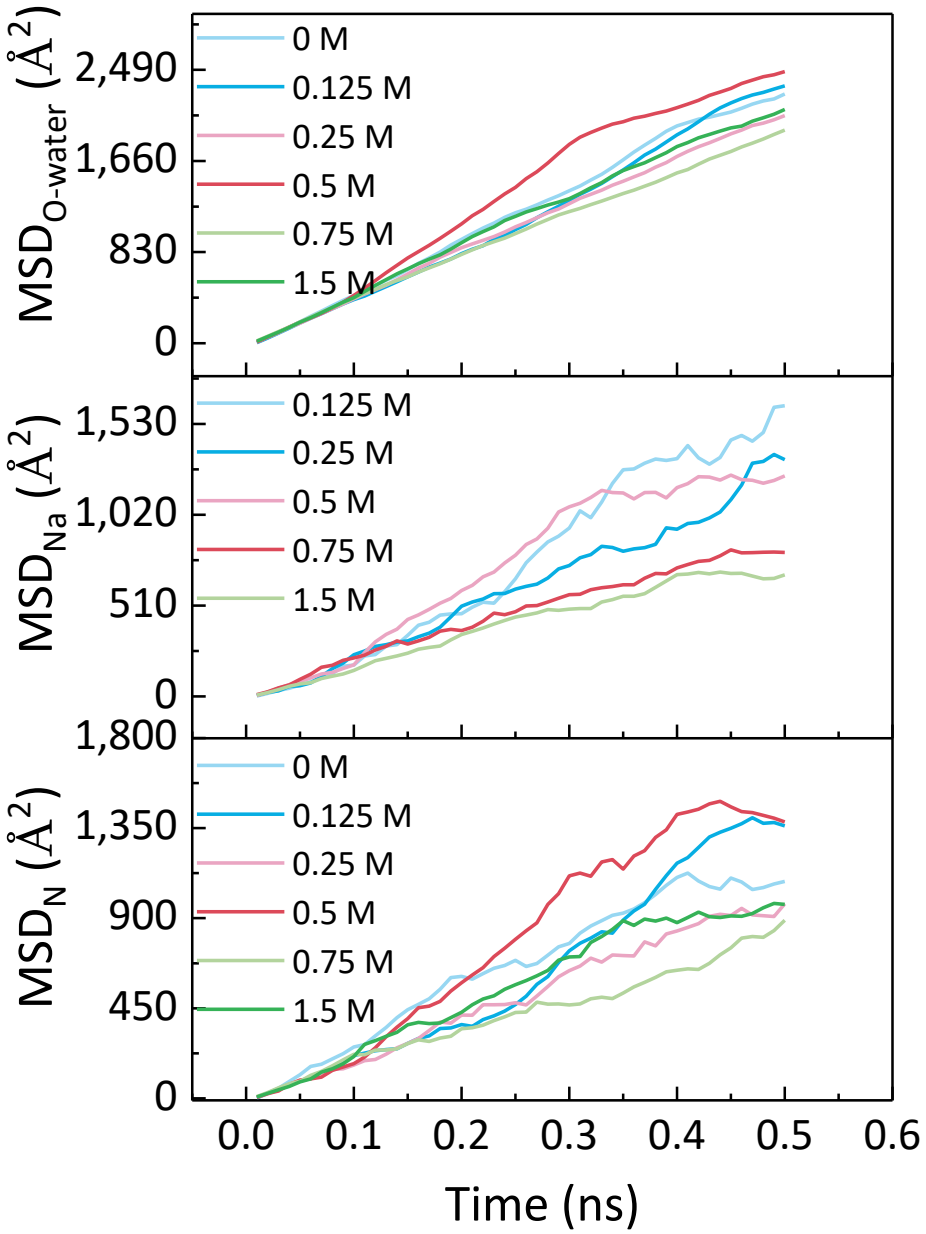
MSD$_{O\text{-}water}$ (Å^2)
2,490
1,660
830
0
0 M
0.125 M
0.25 M
0.5 M
0.75 M
1.5 M
MSD$_{Na}$ (Å^2)
1,530
1,020
510
0
0.125 M
0.25 M
0.5 M
0.75 M
1.5 M
MSD$_N$ (Å^2)
1,800
1,350
900
450
0
0 M
0.125 M
0.25 M
0.5 M
0.75 M
1.5 M
0.0
0.1
0.2
0.3
0.4
0.5
0.6
Time (ns)

(a)

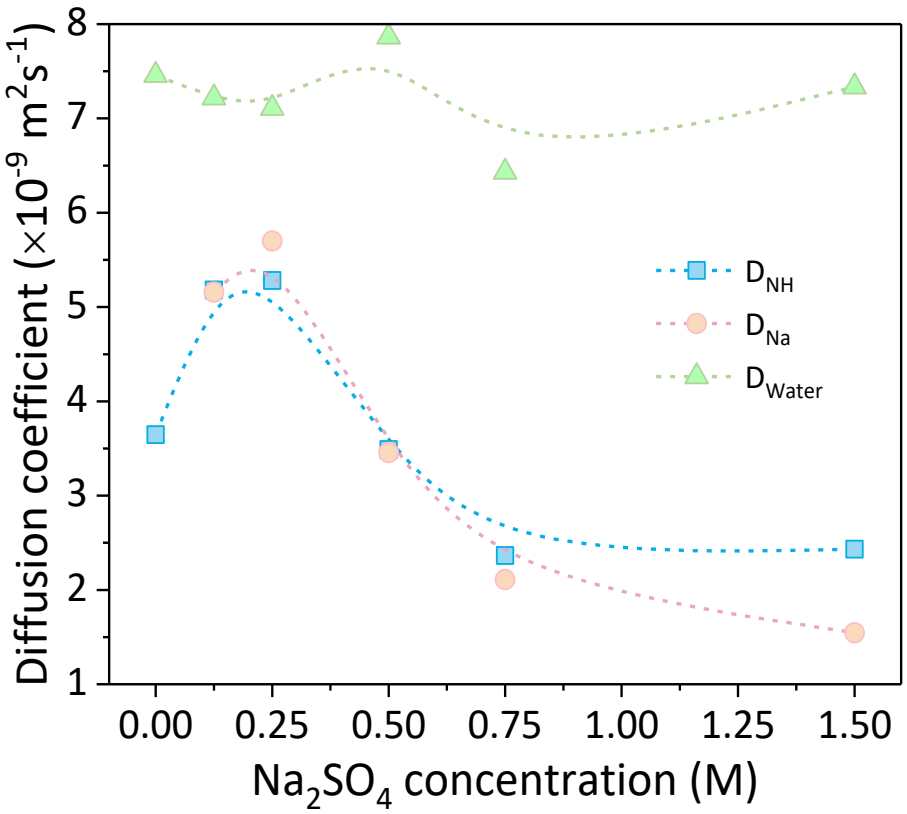

(b)

Figure 3 (a) MSD values of N, Na and O-water in 0.5 ns; (b) diffusion rates of NH_4^+, Na^+ and H_2O molecules as a function of Na2SO4 concentration.

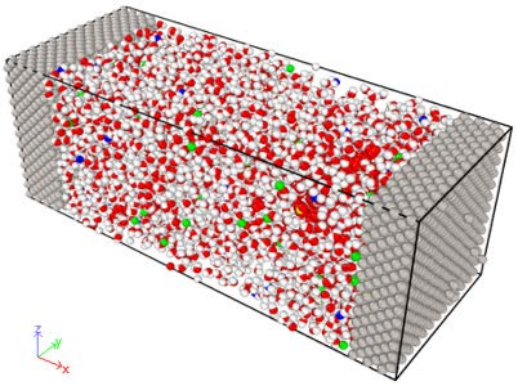

(a)

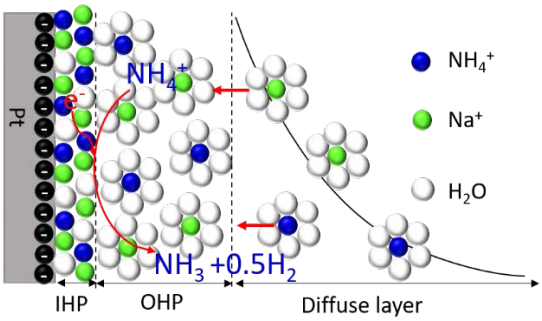
Pt
NH_4^+
e^-
NH_3 +0.5H_2
IHP
OHP
Diffuse layer
NH_4^+
Na^+
H_2O

(b)

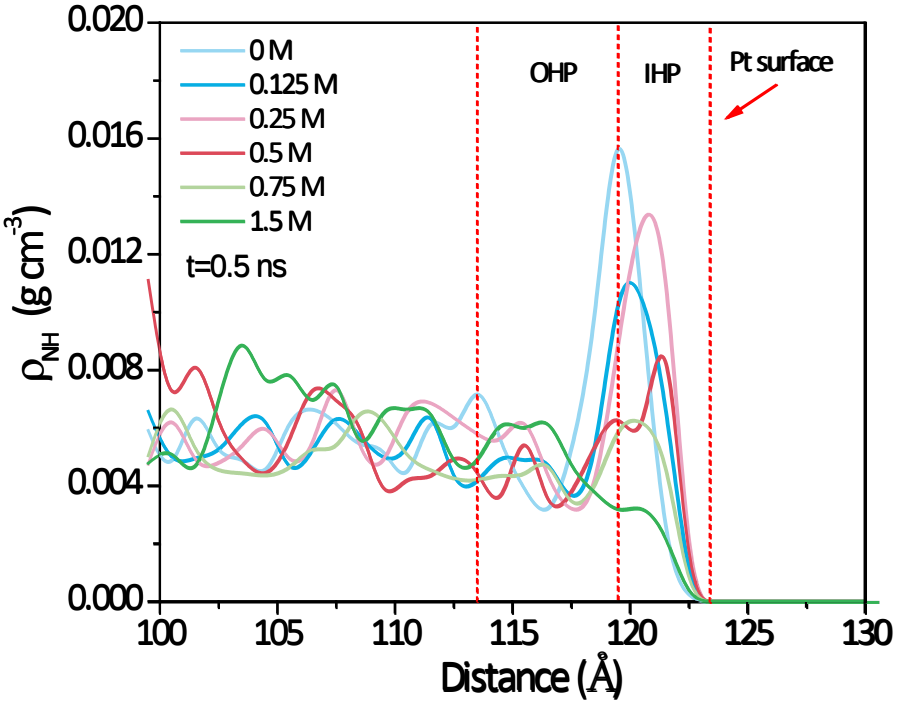
0.020
0.016
0.012
0.008
0.004
0.000
ρ_{NH} (g cm^{-3})
0 M
0.125 M
0.25 M
0.5 M
0.75 M
1.5 M
t=0.5 ns
OHP
IHP
Pt surface
100
105
110
115
120
125
130
Distance (Å)

(c)

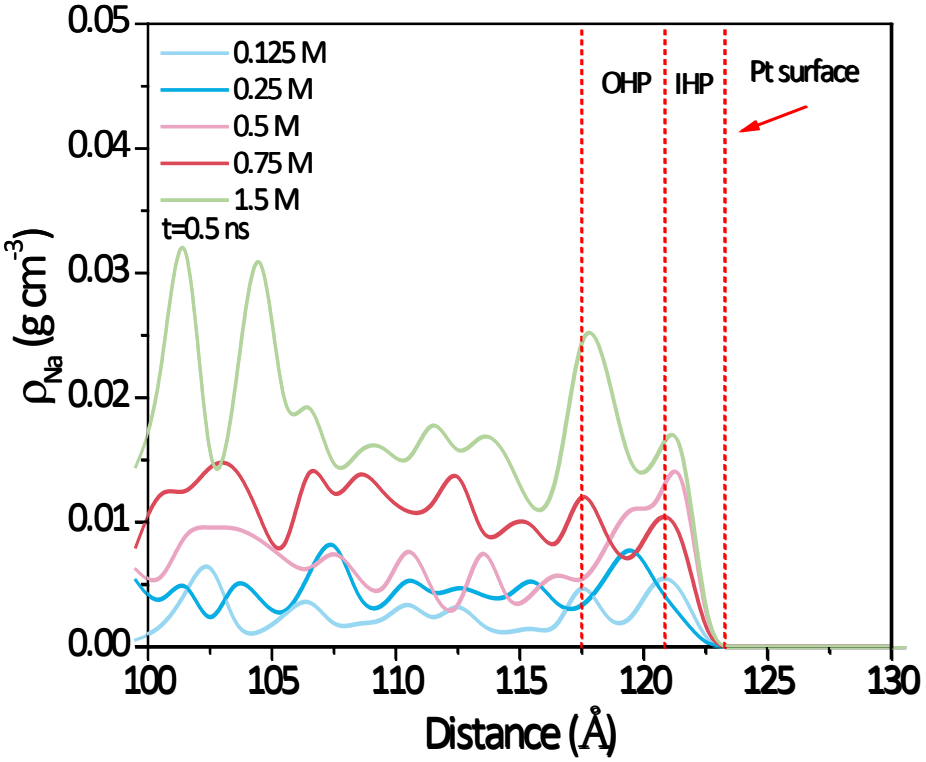

(d)

Figure 4 (a) Single channel model of electrodeionization; (b) NH_4^+ EDL film; (c) and (d) concentration profiles of NH_4^+ and Na^+ as a function of Na_2SO_4 concentration (0–1.5 M).

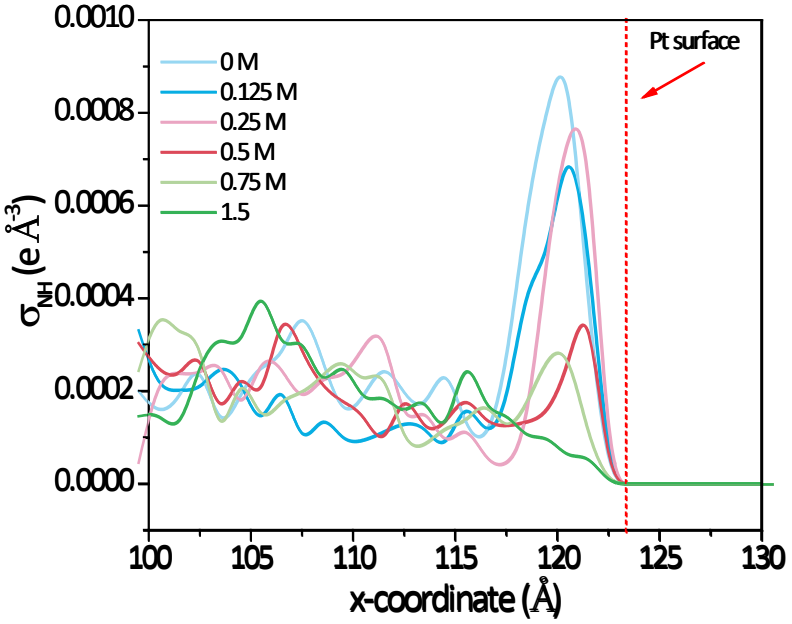
0.0010
0.0008
0.0006
0.0004
0.0002
0.0000
σ_{NH} (e Å^{-3})
0 M
0.125 M
0.25 M
0.5 M
0.75 M
1.5
Pt surface
100
105
110
115
120
125
130
x-coordinate (Å)

(a)

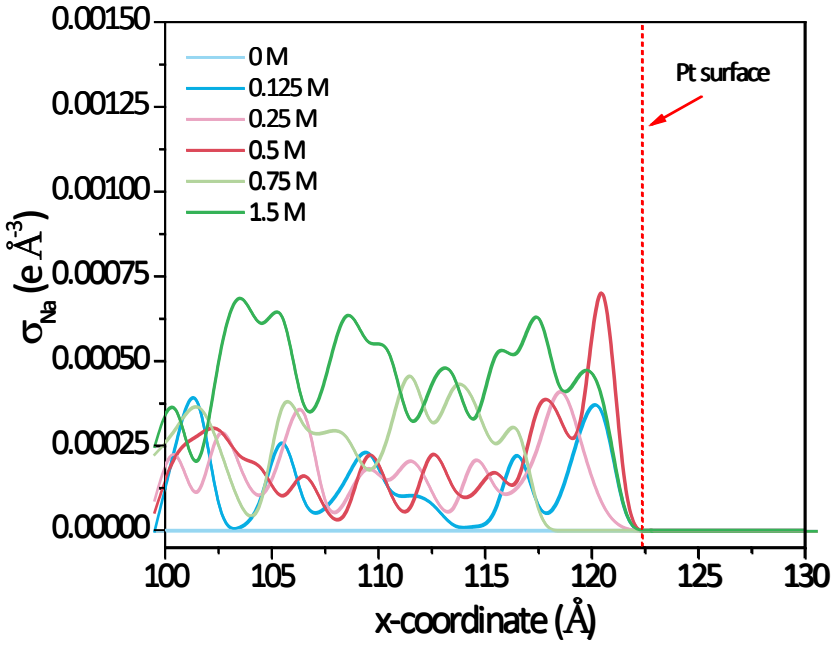
0.00150
0.00125
0.00100
0.00075
0.00050
0.00025
0.00000
σ_{Na} (e Å^{-3})
0 M
0.125 M
0.25 M
0.5 M
0.75 M
1.5 M
Pt surface
100
105
110
115
120
125
130
x-coordinate (Å)

(b)

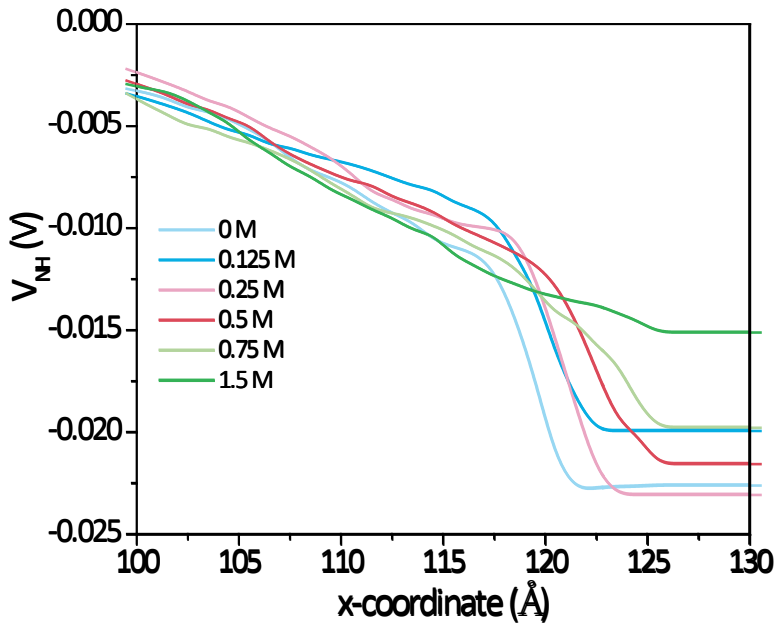

(c)

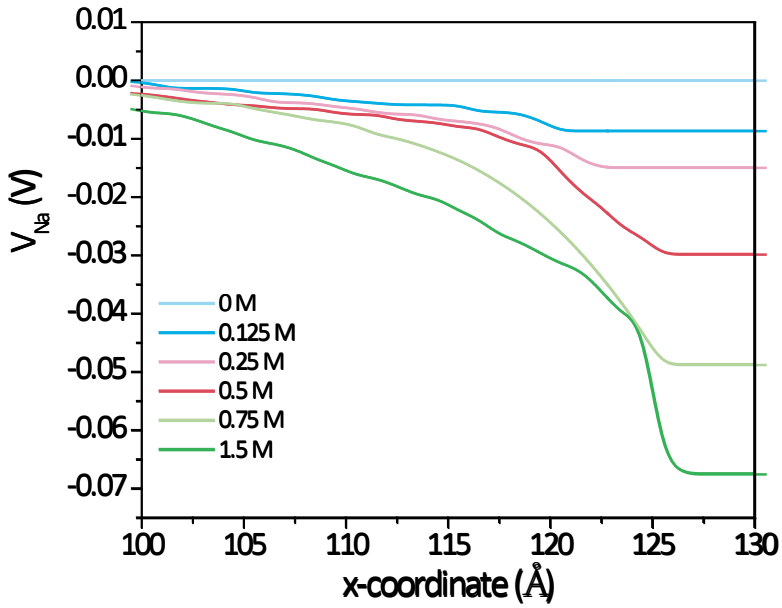

(d)

Figure 5 (a) and (b) Charge density distributions; (c) and (d) potential drops of NH_4^+ and Na^+ along the x-axis under 0–1.5 M Na_2SO_4.

Figure 5 (a) and (b) Charge density distributions; (c) and (d) potential drops of NH_4^+ and Na^+ along the x-axis under 0–1.5 M Na_2SO_4.

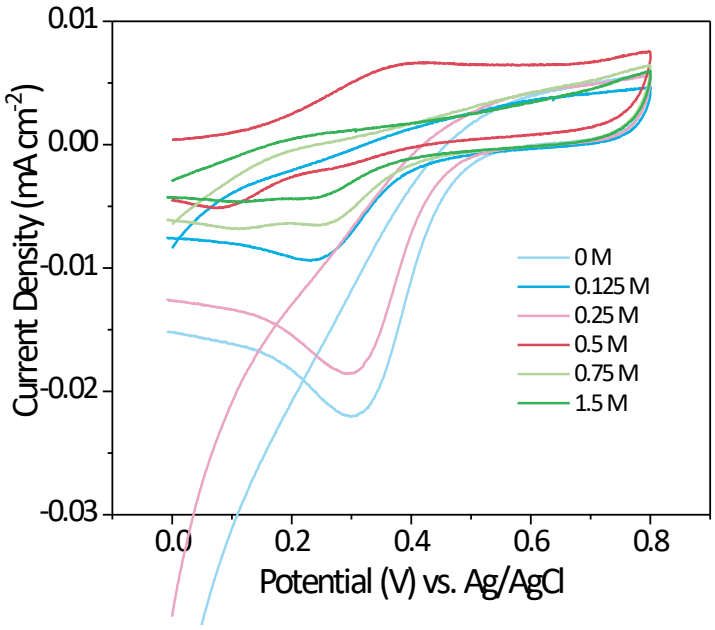

(a)

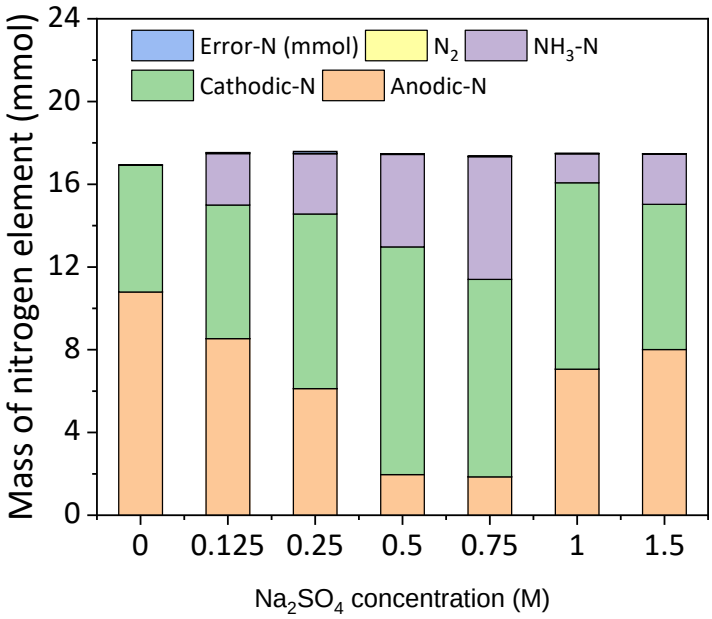

(b)

Figure 6 (a) Current-Voltage curves at 0–1.5 M Na_2SO_4; (b) Nitrogen constituents.

Tables

Table 1 Mobility and transport numbers of NH_4^+, Na^+ and SO_4^{2-} at 0–1.5 M Na_2SO_4

Na_2SO_4 concentration mol L^{-1}	Mobility $\times 10^{-8}$ m^2 V^{-1} s^{-1}			Transport number		
	NH_4^+	Na^+	SO_4^{2-}	NH_4^+	Na^+	SO_4^{2-}
0	1.01	-	3.29	0.67	-	0.33
0.125	1.49	4.06	2.03	0.17	0.33	0.50
0.25	1.33	3.40	1.70	0.17	0.42	0.41
0.50	1.29	2.78	1.39	0.11	0.63	0.26
0.75	1.34	2.45	1.22	0.11	0.63	0.26
1.00	1.37	1.87	0.93	0.08	0.65	0.27
1.50	1.27	1.63	0.81	0.08	0.64	0.28

Table 2 Electric properties of NH_4^+ film and EDL capacitance via MD

Na_2SO_4 concentration mol L^{-1}	Charge density e $Å^{-3}$				Potential drop V				EDL capacitance
	NH_4^+	Na^+	H_2O	Total	NH_4^+	Na^+	H_2O	Total	$\times 10^{-19}$ F $Å^{-3}$
0	0.0041	0.0000	-0.0030	0.0011	-0.0226	0.0	0.0321	0.0095	0.1795
0.125	0.0030	0.0013	-0.0083	-0.0040	-0.0220	-0.0086	0.0252	-0.0054	1.1920
0.25	0.0026	0.0015	-0.0125	-0.0083	-0.0230	-0.0149	0.0231	-0.0149	0.8939
0.5	0.0016	0.0024	-0.0235	-0.0194	-0.0215	-0.0298	0.0262	-0.0251	1.2363
0.75	0.0013	0.0010	-0.0312	-0.0290	-0.0198	-0.0487	0.0276	-0.0409	1.1321
1.5	0.0006	0.0031	-0.0265	-0.0228	-0.0151	-0.0645	0.0347	-0.0449	0.8117

Table 3 EDL structures and thicknesses (NH_4^+ and Na^+) via MD

Na_2SO_4 concentration mol L^{-1}	NH_4^+ layer			Na^+ layer			Total thickness
				Å			
	IHP	OHP	DL	IHP	OHP	DL	
0	6.0	7.5	5.5	--	--	--	19.0
0.125	5.5	8.0	6.0	4.5	4.0	7.5	19.5
0.25	5.5	8.5	7.0	6.0	6.0	6.5	21.0
0.5	5.0	7.0	5.0	8.5	8.5	7.0	24.0
0.75	5.0	6.5	6.0	8.0	7.0	6.0	21.0
1.5	4.0	6.5	5.5	7.5	8.5	7.5	23.5